4
Dissociation Chemistry of Formyl Halides

Unimolecular dissociation chemistry of formyl halides (see Figure 4.1) in gas phase has gained considerable attention. These halogen substituted analogues of formaldehyde are produced in troposphere by degradation of hydrochlorofluorocarbons [Ravishankara *et al.*, 1994]. Dissociation of formyl halides can result in molecular products (HX + CO) and radical products (H, X, XCO, and HCO) which play an important role in stratospheric ozone depletion [Navarro *et al.*, 2015]. Relative rate techniques have been used to estimate a lower limit of 10 years for the atmospheric lifetime of formyl fluoride with respect to its reaction with radicals [Wallington and Hurley, 1993]. In recent years, the presence of HFCO in the atmosphere has been rising due to the increase of the refrigerant HFC-134a concentrations [Xiang *et al.*, 2014]. Kinetic studies of HClCO reaction with H to estimate the atmospheric lifetime of HClCO have been performed [Li and Luo, 2003]. Dowideit et al. [Dowideit *et al.*, 1996] have reported rapid HClCO decay to HCl + CO in aqueous solution with a rate constant of 10^4 s^{-1}. Possible dissociation channels of formyl halides are given in Figure 4.2. Paths (1) and (2) are homolytic dissociations resulting in radical products and the remaining three pathways lead to molecular products. Path (3) is concerted elimination and paths (4) and (5) involve isomer formation via 1,2-X and 1,2-H shift, respectively, followed by dissociation. Electronic structure studies [Kamiya and Morokuma, 1991; Francisco and Zhao, 1992] have shown that path (3) has the lowest energy barrier in the ground state.

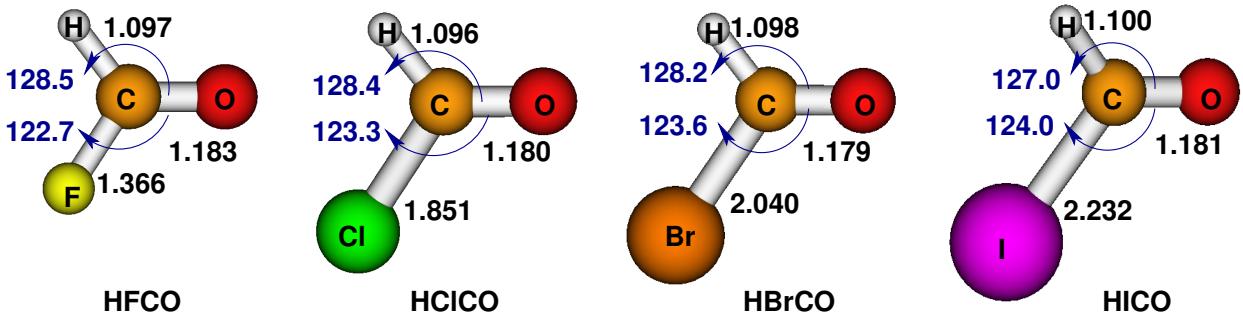

Figure 4.1. : Schematic represenatation of formyl halide molecules HXCO (X = F, Cl, Br and I). All bond lengths and bond angles are computed using B3LYP/6-31G*/ECP level of theory.

Among the formyl halides, HFCO has been investigated in detail and a limited number of studies are available for the other three molecules. Over the years, formyl fluoride has been subjected to several spectroscopic [Choi and Moore, 1989; Choi *et al.*, 1990; Choi and Moore, 1991, 1992, 1995; Saito *et al.*, 1985; Wang *et al.*, 2009; Lee *et al.*, 2005; Reed *et al.*, 1997] and theoretical [Fang and Liu, 2001b; Pasin *et al.*, 2006; Yamamoto and Kato, 1998, 2000; Pradhan and Brown, 2016b; Yamamoto and Kato, 1997; Budenholzer and Yu, 1998; Wei and Wyatt, 1993; Anand and Schlegel, 2002; Viel and Leforestier, 2000; Iung and Ribeiro, 2005; Pradhan and Brown, 2016a] investigations. Electronic structure calculations characterizing the dissociation of HFCO in the ground and excited states have been reported. A full six-dimensional analytic potential energy surface of HFCO based on neural network exponential fitting functions was reported by Pradhan et al. [Pradhan and

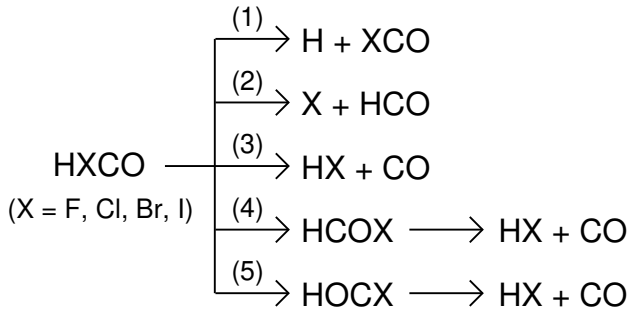

Figure 4.2. : Various dissociation pathways of formyl halides.

Brown, 2016b,a]. The fitting was performed using CCSD(T) data and the fit was accurate up to 10000 cm^{-1} above the zero point level. In addition to electronic structure theory, classical trajectory simulations of HFCO dissociation have been performed. Anand et al. [Anand and Schlegel, 2002] have reported direct classical trajectory studies of $HXCO \longrightarrow HX + CO$ (X = F, Cl) reaction. Trajectories were launched from the transition state on the concerted path (3) and product energy distributions were analyzed. HX fragments showed significant vibrational excitations whereas CO fragment was rotationally excited. Using analytic potential energy functions, trajectory simulations of $HFCO \longrightarrow HF + CO$ reaction were carried out by Yamamoto et al. [Yamamoto and Kato, 1997] and Budenholzer et al. [Budenholzer and Yu, 1998]. These studies showed mode specific effects and incomplete intramolecular vibrational energy redistribution (IVR) even above the dissociation limit. Excitation of the CH stretch enhanced the dissociation rate and excitation of CO stretch or any of the out-of-plane modes resulted in smaller rates. Quantum dynamics calculations investigating similar aspects of HFCO dissociation have also been reported. These calculations were performed using planar four and five dimensional models [Yamamoto and Kato, 1998] and a full six-dimensional model [Yamamoto and Kato, 2000]. These dynamics studies were primarily focused on the concerted path (3) to form HX + CO. On the experimental side, Moore and co-workers have investigated the dissociation dynamics of vibrationally excited HFCO using stimulated emission pumping technique [Choi and Moore, 1989; Choi *et al.*, 1990; Choi and Moore, 1991, 1992, 1995]. They identified strongly state specific unimolecular reaction rates and mode dependent dynamics in agreement with above mentioned theoretical studies.

Formyl chloride (HClCO) is a reactive intermediate in the decomposition of several chlorinated hydrocarbons. Equilibrium structure of formyl chloride was identified in a microwave spectroscopic experiment [Davis and Gerry, 1983]. Francisco et al. [Francisco and Zhao, 1992] characterized the dissociation pathways of HClCO using unrestricted Møller-Plesset perturbation theory using split-valence and polarized basis sets. They predicted a barrier height of 37.8 kcal/mol for the $HClCO \longrightarrow HCl + CO$ reaction while Tyrrell et al. [Tyrrell and Lewis-bevan, 1992] predicted 44.0 kcal/mol using MP2/6-31G** theory. Vertical excitation energies of HClCO have been computed using QCISD(T) and density functional theory calculations [Bent *et al.*, 1994]. Multi-reference theories have been used to characterize the radical paths (1) and (2) in the ground and lower excited states of HClCO [Mu and Gruber-Stadler, 2008; Fang and Liu, 2001a]. Unlike the two molecules discussed above, studies on HBrCO and HICO are limited. HBrCO has been identified as an intermediate in many gas phase reactions and its dissociation has been invoked in several reaction schemes [Yarwood *et al.*, 1991a; Timonen *et al.*, 1988; Barnes *et al.*, 1989; Leitzke *et al.*, 2003]. Chu et al. [Lin *et al.*, 1999] found the B3LYP/6-31G* level of theory to be reasonably good in describing the structures of HICO. Infrared spectroscopic investigation of formyl bromide was performed by Yarwood et al. [Yarwood *et al.*, 1991b] and formyl iodide by Barnes et al.

[Barnes *et al.*, 1995]. Electronic structure calculations of dissociation energy profile of HBrCO at PMP4SDTQ theory predicted [Zhao and Francisco, 1992] a barrier height of 31.0 kcal/mol for the primary molecular pathway (3).

4.1 COMPUTATIONAL METHODOLOGY

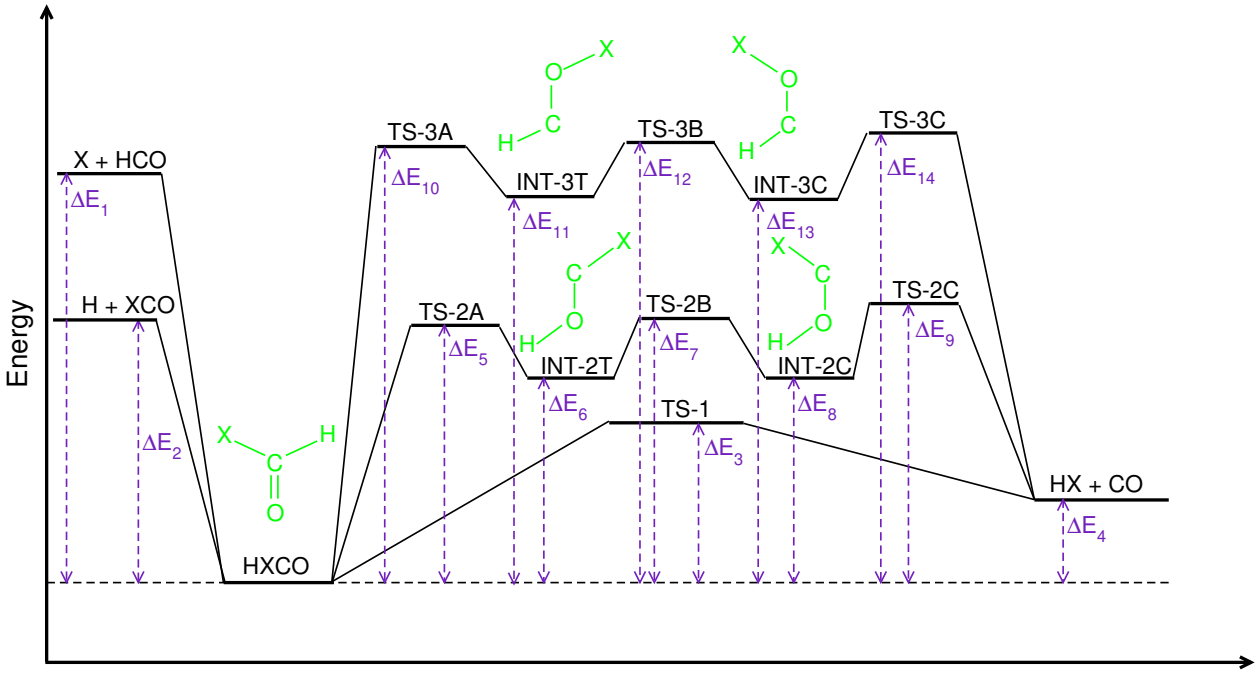

Figure 4.3. : Schematic describing the energy profiles of formyl halides. Values of ΔE_1, ΔE_2, etc., computed using B3LYP/6-31G*/ECP are given in Table 4.1.

Stationary points on the potential energy surfaces of HXCO molecules were characterized using density functional B3LYP/6-31G* level of electronic structure theory with LANL2DZ effective core potentials (ECP) for the halogen atoms [Feller, 1996; Schuchardt *et al.*, 2007; Wadt and Hay, 1985]. This level of theory was chosen because it was accurate enough to capture the features of the HXCO potential energy surface and small enough that it was computationally feasible to produce an appreciable number of direct dynamics trajectories. All the stationary points were geometry optimized and frequency calculations were carried out to identify transition states (TSs). Intrinsic reaction coordinate calculations were performed to make sure that a given TS connects the correct product(s) with the reactant. A schematic showing the energy profile of formyl halides is given in Figure 4.3. The quantities TS-2A, INT-2T, etc. present in the figure are described below.

1. Path (1)
   $HXCO \xrightarrow{\Delta E_2} H + XCO$

   - ΔE_2 is the electronic energy of H + XCO relative to HXCO.

2. Path (2)
   $HXCO \xrightarrow{\Delta E_1} X + HCO$

   - ΔE_1 is the electronic energy of X + HCO relative to HXCO.

3. Path (3) HXCO $\xrightarrow{\Delta E_3}$ TS-1 $\xrightarrow{\Delta E_4}$ HX + CO

   - ΔE_3 is the electronic energy of TS-1 relative to HXCO.
   - ΔE_4 is the electronic energy of HX + CO relative to HXCO.

4. Path (4)
   HXCO $\xrightarrow{\Delta E_{10}}$ TS-3A $\xrightarrow{\Delta E_{11}}$ INT-3T(trans-HCOX) $\xrightarrow{\Delta E_{12}}$ TS-3B $\xrightarrow{\Delta E_{13}}$
   INT-3C(cis-HCOX) $\xrightarrow{\Delta E_{14}}$ TS-3C $\xrightarrow{\Delta E_4}$ HX + CO

   - ΔE_{10} is the electronic energy of TS-3A relative to HXCO. TS-3A is the transition state connecting HXCO with trans-HCOX following 1,2-X shift.
   - ΔE_{11} is the electronic energy of INT-3T relative to HXCO. INT-3T represents trans-HCOX.
   - ΔE_{12} is the electronic energy of TS-3B relative to HXCO. TS-3B is the transition state connecting trans-HCOX with cis-HCOX.
   - ΔE_{13} is the electronic energy of INT-3C relative to HXCO. INT-3C represents cis-HCOX.
   - ΔE_{14} is the electronic energy of TS-3C relative to HXCO. TS-3C is the transition state connecting cis-HCOX with HX + CO.
   - ΔE_4 is the electronic energy of HX + CO relative to HXCO.

5. Path (5)
   HXCO $\xrightarrow{\Delta E_5}$ TS-2A $\xrightarrow{\Delta E_6}$ INT-2 T(trans-HOCX) $\xrightarrow{\Delta E_7}$ TS-2B $\xrightarrow{\Delta E_8}$
   INT-2C(cis-HOCX) $\xrightarrow{\Delta E_9}$ TS-2C $\xrightarrow{\Delta E_4}$ HX + CO

   - ΔE_5 is the electronic energy of TS-2A relative to HXCO. TS-2A is the transition state connecting HXCO with trans-HOCX following 1,2-H shift.
   - ΔE_6 is the electronic energy of INT-2T relative to HXCO. INT-2T represents trans-HOCX.
   - ΔE_7 is the electronic energy of TS-2B relative to HXCO. TS-2B is the transition state connecting trans-HOCX with cis-HOCX.
   - ΔE_8 is the electronic energy of INT-2C relative to HXCO. INT-2C represents cis-HOCX.
   - ΔE_9 is the electronic energy of TS-2C relative to HXCO. TS-2C is the transition state connecting cis-HOCX with HX + CO.
   - ΔE_4 is the electronic energy of HX + CO relative to HXCO.

ΔE_1, ΔE_2, etc. are electronic energies (without zero point corrections) computed using B3LYP/6-31G* level of electronic structure theory with LANL2DZ effective core potentials for the halogen atoms. The 1,2-X shift [leading to HCOX, path(4)] occurs via TS-3A and the 1,2-H shift [to HOCX, path(5)] involves TS-2A. These shifts result in the formation of trans isomers (INT-3T and INT-2T) followed by isomerization to the corresponding cis isomers (INT-3C and INT-2C) and subsequent dissociation to HX + CO products. The quantities ΔE_1, ΔE_2, etc., given in Figure 4.3 are electronic energies of various species relative to the reactant HXCO. Values of ΔE_1, ΔE_2, etc.,

Table 4.1. : Stationary point energies (in kcal/mol) of HXCO (X = F, Cl, Br, and I) potential energy surface computed using B3LYP/6-31G*/ECP theory. Energies are relative to the reactant HXCO molecule and are without zero point energy corrections.

	HFCO	HClCO	HBrCO	HICO
ΔE_1 (X + HCO)	117.2	79.5	66.2	54.2
ΔE_2 (H + XCO)	105.9	94.6	85.6	77.3
ΔE_3 (TS-1)	52.8	35.9	33.7	33.5
ΔE_4 (HX + CO)	20.1	10.8	10.0	8.4
ΔE_5 (TS-2A)	84.2	84.5	83.5	82.8
ΔE_6 (INT-2T)	48.9	52.5	52.7	52.9
ΔE_7 (TS-2B)	68.6	70.3	69.1	69.0
ΔE_8 (INT-2C)	48.6	51.1	51.0	51.8
ΔE_9 (TS-2C)	73.4	64.3	63.1	63.6
ΔE_{10} (TS-3A)	111.7	77.9	70.4	116.0
ΔE_{11} (INT-3T)	111.1	76.5	68.5	62.6
ΔE_{12} (TS-3B)	111.7	78.5	71.6	67.1
ΔE_{13} (INT-3C)	99.3	65.3	57.5	52.0
ΔE_{14} (TS-3C)	101.2	68.2	61.3	56.7

computed using B3LYP/6-31G*/ECP are given in Table 4.1. These are classical energies without zero point corrections. A comparison of these values with benchmark CCSD(T) calculations are given in Annexure A. The CCSD(T) single point energies were calculated using geometries optimized at the MP2/6-31G*/ECP level of theory. Also, a comparison of the B3LYP/6-31G*/ECP values with previously reported studies is given in Annexure A. Using the barrier heights and frequencies computed from the B3LYP/6-31G*/ECP theory, RRKM rate constants for the dissociation of formyl halides were calculated using standard procedures [Zhu and Hase, 1994].

To establish atomic level dissociation mechanisms of formyl halides, Born-Oppenheimer direct chemical dynamics simulations [Paranjothy *et al.*, 2013; Sun and Hase, 2003] were performed at fixed total energies E_{tot}. The simulations were performed at two different total energies - a high energy simulation (E_{tot} = 200 kcal/mol for all four molecules) and a low energy simulation (E_{tot} = 130, 100, 90, and 120 kcal/mol, for X = F, Cl, Br, and I, respectively). The lower energy values were selected such that the molecules have total energy slightly above the highest barrier in the corresponding potential energy surface. The energies were distributed among the normal modes of the molecules using classical micro-canonical sampling algorithm [Peslherbe *et al.*, 1999]. No rotational energy was added to the molecules. The trajectories were launched from the reactant well and propagated till 4 ps or until dissociation occurred and the products reached a separation of 10.0 Å. The integrations were performed using a 6^{th} order Symplectic integrator [Schlier and Seiter, 2000, 1998] with a step size of 0.5 fs. These conditions were sufficient to achieve good energy conservation in the trajectories. E_{tot} as a function of time for a few trajectories is given in Figure 4.4. Total energy in the classical trajectories reported here was conserved within $E_{tot} \pm 1.0$ kcal/mol.

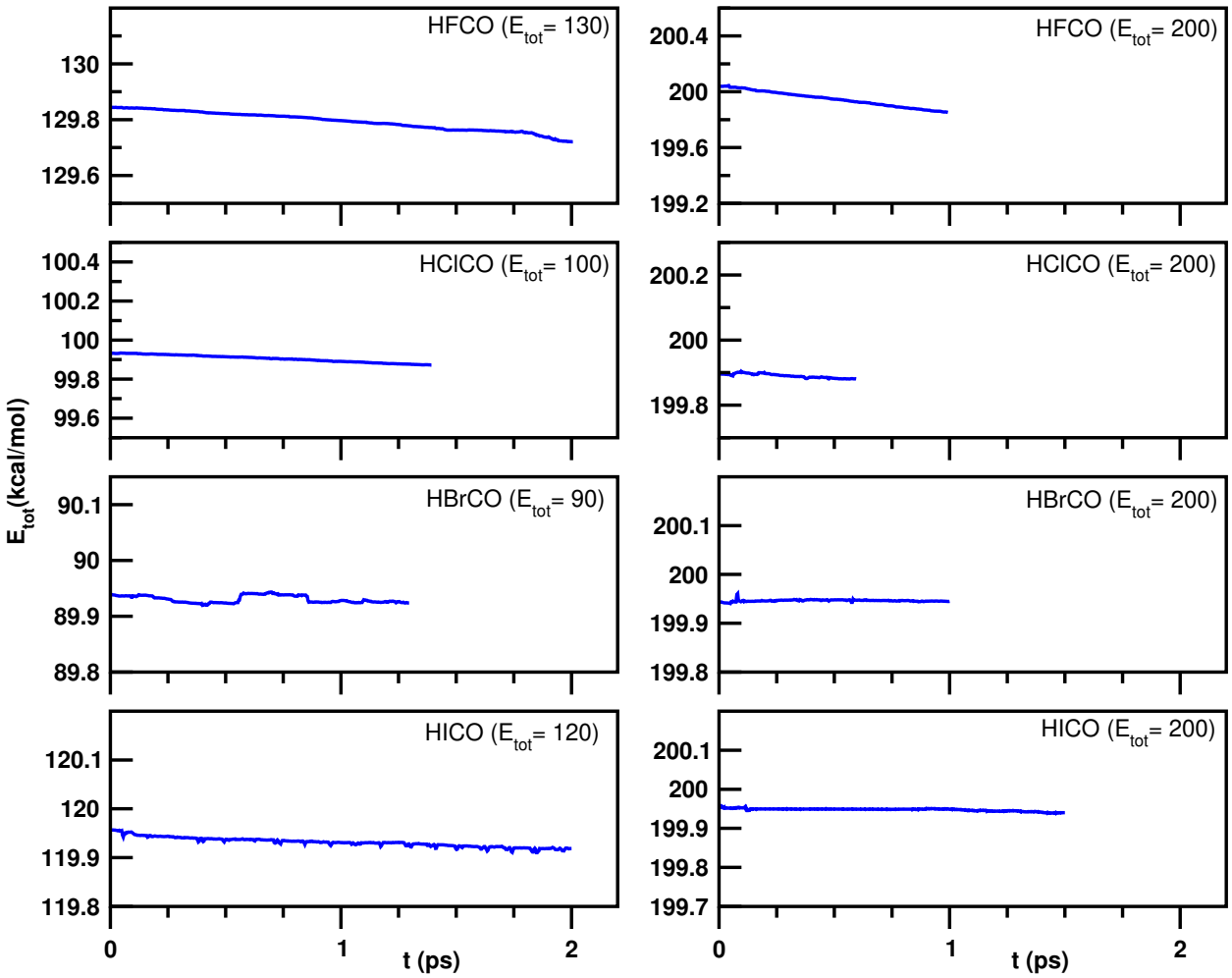

Figure 4.4. : Total energy E_{tot} as a function of time for a few sample classical trajectories. In all plots, x-axes ranges are same.

4.2 RESULTS AND DISCUSSION

4.2.1 Potential Energy Surface

Shape of the potential energy curves are similar for all the four molecules with differences in the energetics. Some general aspects of the energy profiles of formyl halides are briefly discussed here. The radical pathways (1) and (2) do not have barriers above the reaction endothermicities in agreement with previous studies [Fang and Liu, 2001b,a; Zhao and Francisco, 1992]. The radical dissociation energies decrease in going from F to I (see Table 4.1). This decrease is more enhanced for C−X cleavages in comparison to C−H dissociations. For the former, energy decreases from 117.2 kcal/mol (C−F) to 54.2 kcal/mol (C−I) and for the latter, energies range from 105.9 kcal/mol (C−F) and 77.3 kcal/mol (C−I). The C-X bond strength increases while moving from I to F due to the increase in ionic character and coulombic stabilization. In HFCO, the C-X bond energy is greater than the C-H energy while the reverse is true for the other three halides. Liu et al. [Fang and Liu, 2001b,a] have reported CASSCF calculations characterizing the radical dissociations for the HFCO and HClCO molecules. For HFCO, zero point energy corrected dissociation energies [Fang and Liu, 2001b] (CAS(8,7)/cc-pVTZ) for C-F and C-H bonds are 109.8 and 101.0 kcal/mol, respectively. The present calculations (B3LYP/6-31G*/ECP) showed bond energies of 112.3 (C-F) and 97.9 kcal/mol (C-H). Experimental estimations [Maul *et al.*, 1999] for

Table 4.2. : Imaginary frequencies (in cm^{-1}) associated with the transition states of all the four molecules computed using B3LYP/6-31G*/ECP theory.

transition state	HFCO	HClCO	HBrCO	HICO
TS-1 HXCO → HX + CO (concerted path)	-1485	-1065	-1049	-1075
TS-2A HXCO → trans-HOCX (INT-2T)	-1918	-1934	-1942	-1956
TS-2B trans-HOCX (INT-2T) → cis-HOCX (INT-2C)	-1918	-1934	-1942	-1956
TS-2C cis-HOCX (INT-2C) → HX + CO	-1573	-1160	-1180	-1213
TS-3A HXCO → trans-HCOX (INT-3T)	-490	-384	-404	-1133
TS-3B trans-HCOX (INT-3T) → cis-HCOX (INT-3C)	-746	-721	-796	-868
TS-3C cis-HCOX (INT-3C) → HX + CO	-479	-404	-414	-423

the C-F and C-H dissociation energies are 115.3 and 100.0 kcal/mol, respectively. For HClCO, CASMP2/cc-pVTZ//CAS(8,7)/cc-pVTZ computed energies [Fang and Liu, 2001a] are 90.0 (C-Cl) and 95.4 kcal/mol (C-H). The present computed values are 75.7 (C-Cl) and 86.5 kcal/mol (C-H). Further, an MRD-CI study [Mühlhäuser and Gruber-Stadler, 2008] of HClCO → Cl + HCO predicted a dissociation energy of 76.1 kcal/mol. For the C-H dissociation of HClCO, Becker et al. [Libuda *et al.*, 1990] estimated 91.5 kcal/mol of energy from experimental and theoretical heats of formation.

The molecular products HX + CO can result via three different pathways as shown in Figure 4.3. The concerted path (via TS-1) has the lowest barrier and the other two pathways occurring via isomerizations have higher overall energy requirements (∼84 kcal/mol for HOCX and slightly above 110 kcal/mol for HCOX isomerization, see Table 4.1) and may not be accessible at room temperature. These predictions are in consistent with previous investigations [Zhao and Francisco, 1992; Lin *et al.*, 1999; Morokuma *et al.*, 1980; Goddard and Schaefer, 1990] and the present benchmark CCSD(T) results present in the Annexure A. TS energies for the concerted pathway (ΔE_3) vary from 33 to 53 kcal/mol whereas barriers lie between 70-116 kcal/mol for the 1,2-X shift and 82-85 kcal/mol for the 1,2-H shift. These isomerizations first lead to the respective trans structures (INT-2T and INT-3T) which undergo H rotation to the corresponding cis configurations (INT-2C and INT-3C) which is followed by dissociation. In general, the H migrated carbenes (HOCX, via TS-2A) are more stable than the corresponding X migrated species (HCOX, via TS-3A). ΔE_5 for the 1,2-H shift has small variations in moving from F to I indicating no substitution effect for the proton transfer pathway. Similar trends are observed for other stationary points in this path (ΔE_6, ΔE_7, ΔE_8) except for the final dissociation transition state (ΔE_9, TS-2C). On the other hand, stationary point energies in the 1,2-X pathway show considerable variations depending upon the substituent. These trends are also reflected in the imaginary frequencies associated with the respective TSs (shown in Table 4.2). For the proton transfer pathways, the frequencies are in the range of 1918-1956 cm^{-1} (TS-2A) and for the the X transfer, frequencies vary between 490-1132

cm^{-1} (TS-3A). The high imaginary frequencies for the proton transfer indicate possible tunneling contributions.

Table 4.3. : B3LYP/6-31G*/ECP computed energies of the trans → cis isomerization pathways of HCOX isomers. Energies are in kcal/mol and relative to reactant HXCO molecule.

	HXCO	trans-HCOX	inv-TS[a]	tor-TS[b]	cis-HCOX
X=F	0.0	111.1	111.7	192.3	99.3
X=Cl	0.0	76.5	78.5	146.5	65.3
X=Br	0.0	68.5	71.6	131.9	57.5
X=I	0.0	62.6	67.1	115.7	52.0

[a] in-plane inversion transition state (TS-3B), low energy pathway.
[b] out-of-plane torsion transition state, high energy pathway.

Table 4.4. : B3LYP/6-31G*/ECP computed energies of the trans → cis isomerization pathways of HOCX isomers. Energies are in kcal/mol and relative to reactant HXCO molecule.

	HXCO	trans-HOCX	inv-TS[a]	tor-TS[b]	cis-HOCX
X=F	0.0	48.9	182.9	68.6	48.6
X=Cl	0.0	52.5	154.2	70.3	51.1
X=Br	0.0	52.7	128.3	69.1	51.0
X=I	0.0	52.9	119.9	69.0	51.8

[a] in-plane inversion transition state, high energy pathway.
[b] out-of-plane torsion transition state (TS-2B), low energy pathway.

Cis and trans isomers of HOCX have similar energies which was also reported by Francisco et al. [Francisco and Zhao, 1992], for HOCF and HOCCl. But for the HCOX isomers, cis is more stable than the trans form. This is due to the elongated O−X bond distances and reduced steric effects in HCOX in comparison to shorter C−X distances in HOCX. The elongated O−X bond distances in HCOX have been observed in a previous work and it has been suggested that they might be weakly bound complexes [Francisco and Zhao, 1992]. Trans ⟶ cis isomerization of HCOX and HOCX can occur via the H atom *in-plane* inversion or *out-of-plane* torsion about the C−O bond [Sindhu *et al.*, 2019]. In the present calculations, the in-plane inversion path for HCOX and out-of-plane torsion for HOCX were found to be low energy pathways. This has been previously observed for HFCO by Kamiya et al. [Kamiya and Morokuma, 1991], and Francisco et al. [Francisco and Zhao, 1992]. Energetics of the isomerization pathways are presented in Table 4.3 and 4.4. Isomerizations via rotation of halogen atoms have higher energy requirements [Francisco and Zhao, 1992] and attempts were not made to find the corresponding TSs. Optimized geometries of all the species along with relevant bond distances are presented in Figures 4.5 - 4.8. For the HBrCO and HICO molecules, the potential energy profiles with spin-orbit interactions were also computed. The calculations were performed using the spin-orbit corrected ECP for the Br and I atoms proposed by the Stuttgart group [Bergner *et al.*, 1993]. Except for one stationary point (TS-3A, HICO) the differences in the energies with and without the spin-orbit corrections were below 5 kcal/mol. The results are summarized in the Table 4.5. The table below shows comparison of potential energy profiles for the HBrCO and HICO molecules computed using the B3LYP/6-31G*/ECP (Stuttgart group, SO included) and B3LYP/6-31G*/ECP(LANL2DZ)

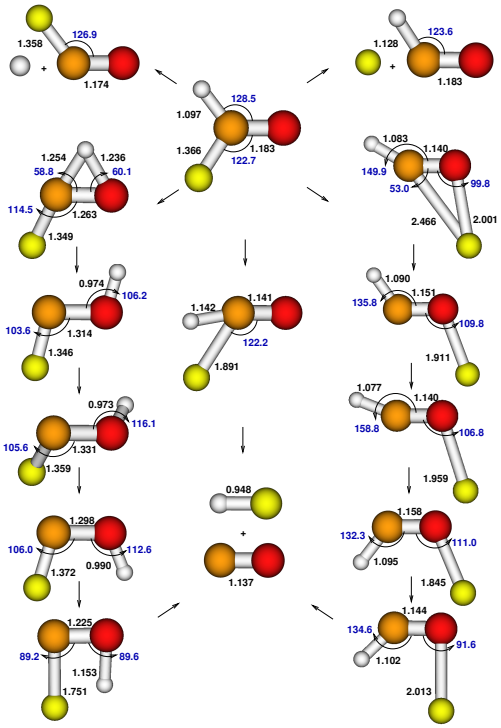

Figure 4.5. : Optimized geometries (B3LYP/6-31G*/ECP) of various stationary points on the potential energy surface of HFCO. Bond distances are in Å and angles are in degrees.

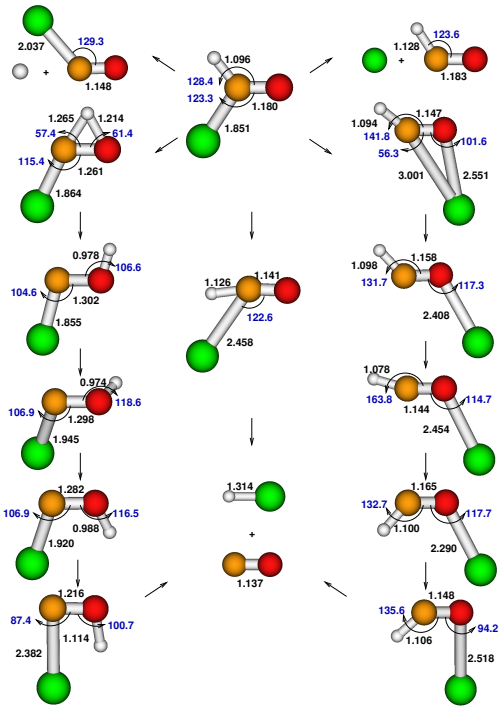

Figure 4.6. : Optimized geometries (B3LYP/6-31G*/ECP) of various stationary points on the potential energy surface of HClCO. Bond distances are in Å and angles are in degrees.

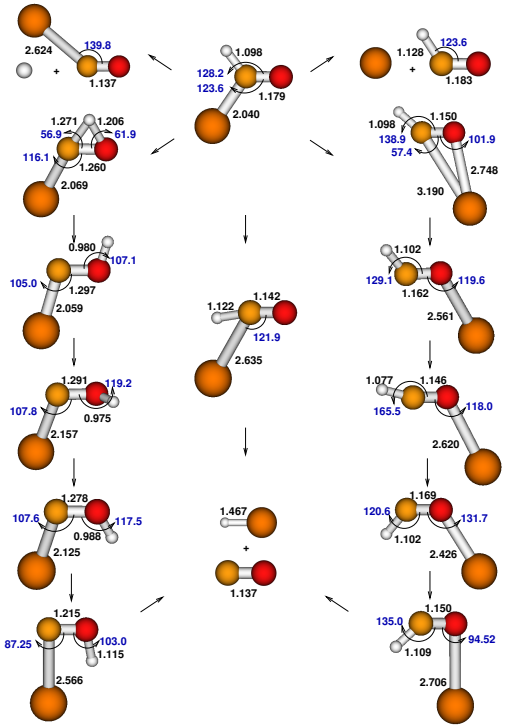

Figure 4.7. : Optimized geometries (B3LYP/6-31G*/ECP) of various stationary points on the potential energy surface of HBrCO. Bond distances are in Å and angles are in degrees.

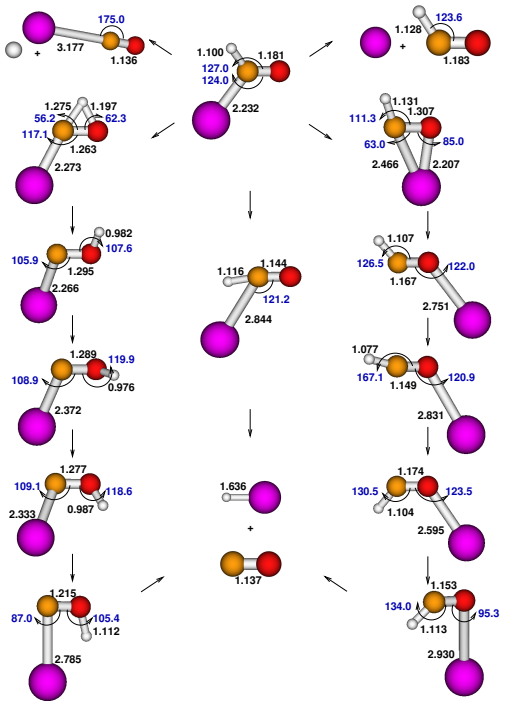

Figure 4.8. : Optimized geometries (B3LYP/6-31G*/ECP) of various stationary points on the potential energy surface of HICO. Bond distances are in Å and angles are in degrees.

theory used for the direct dynamics simulations. The dynamics simulations reported below were performed using the B3LYP/6-31G*/ECP(LANL2DZ) theory without the spin-orbit corrections. In the following section, detailed discussions of the dissociation dynamics of formyl halides are presented.

Table 4.5. : Comparison of potential energy profiles for the HBrCO and HICO species with and without the spin-orbit corrections.

species	B3LYP/6-31G* ECP,Stuttgart (SO included)	B3LYP/6-31G* ECP, LANL2DZ	species	B3LYP/6-31G* ECP, Stuttgart (SO included)	B3LYP/6-31G* ECP, LANL2DZ
HBrCO	0.0	0.0	HICO	0.0	0.0
Br + HCO	62.7	66.2	I + HCO	49.8	54.2
H + BrCO	86.0	85.6	H + ICO	73.2	77.3
TS-1	33.5	33.7	TS-1	33.6	33.5
HBr + CO	11.3	10.0	HI + CO	10.8	8.4
TS-2A	83.3	83.5	TS-2A	82.5	82.8
INT-2T	52.0	52.7	INT-2T	52.2	52.9
TS-2B	68.7	69.1	TS-2B	65.3	69.0
INT-2C	50.8	51.0	INT-2C	51.5	51.8
TS-2C	63.1	63.1	TS-2C	63.6	63.6
TS-3A	68.6	70.4	TS-3A	**61.4**	**116.0**
INT-3T	67.9	68.5	INT-3T	60.7	62.6
TS-3B	69.8	71.6	TS-3B	65.3	67.1
INT-3C	57.0	57.5	INT-3C	50.9	52.0
TS-3C	60.3	61.3	TS-3C	54.6	56.7

4.2.2 Direct Dynamics

In the dynamics simulations, 300 trajectories were generated at a given total energy for each of the four molecules which amounts to 600 trajectories per molecule. The trajectories were classified based on the products observed and a summary is presented in Table 4.6. Clearly, the dominant products were $HX + CO$ in all the simulations. At low energies, exclusively $HX + CO$ products were observed in all the 300 trajectories for X = F, Cl, Br, and in 286 trajectories for X = I. In the high energy (E_{tot} = 200 kcal/mol) simulations, homolytic dissociations resulting in radical products were also observed in addition to the molecular products. Except for HFCO, the $C-X$ dissociations were dominant over the $C-H$ dissociations. This is due to the large C-F bond energy associated with the largest electronegativity of F among all halogens. Simultaneous elimination of H and X over very short time scales were also observed in the high energy simulations of HClCO, HBrCO, and HICO. These are "shattering" type of dissociations [Meroueh *et al.*, 2002] occurring due to the large amounts of energy in the trajectories. Energy profile diagram in Figure 4.3 shows that the molecular products $HX + CO$ can result by three different pathways viz. concerted (via TS-1) and stepwise mechanisms involving HOCX and HCOX isomers. The concerted pathway has the lowest barrier and was observed in a major fraction of trajectories. The isomerization pathways were observed only in small fractions due to high energy barriers. In fact, 1,2-H transfer pathway was observed in 7 (130 kcal/mol) and 28 (200 kcal/mol) trajectories for HFCO and in less than 5 trajectories for the other three molecules. The 1,2-X shift pathway was observed in only one trajectory each in the HFCO and HICO high energy simulations. In addition to these pathways, the molecular products also resulted via an indirect pathway involving radical recombinations in an

Table 4.6. : Number of trajectories yielding a given product following formyl halide decomposition.

	X + HCO	H + XCO	HX + CO	H + X + CO
HFCO				
E_{tot} = 130[a]	0	0	300	0
E_{tot} = 200	9	17	274	0
HClCO				
E_{tot} = 100	0	0	300	0
E_{tot} = 200	51	10	198	41
HBrCO				
E_{tot} = 90	0	0	300	0
E_{tot} = 200	49	13	187	51
HICO				
E_{tot} = 120	14	0	286	0
E_{tot} = 200	68	11	148	73

[a]energy in kcal/mol

appreciable fraction of trajectories. In such trajectories, homolytic dissociations occurred initially resulting in X + HCO and H + XCO products. The radical products did not separate immediately upon formation. The X (H) radical moved away and came back abstracting H (X) resulting in HX + CO products. Figure 4.9 shows the fractions of trajectories resulting in the HX + CO products via the above mentioned three different mechanisms. The quantity f_T is equal to the ratio of number of trajectories for a given pathway and the total number of HX + CO forming trajectories. Major fractions of the trajectories follow the direct pathway (black circles in figure) due to low energy barriers. Indirect trajectories (red squares) contribute to some extent in the high energy simulations as the energy requirements of homolytic dissociations are large. The isomerizations were observed only in a very small fraction of trajectories (blue triangles). In some of the indirect trajectories of HFCO, the F (H) radical moved a long distance away from the central C atom indicating possible roaming mechanism. Roaming of H atom in formaldehyde is well known [Suits, 2008] and here the possibilities of roaming in halogen substituted formaldehydes are shown. Indirect pathway involving C−H dissociation occurred only for HFCO. For the other three molecules, the indirect trajectories showed only C−X dissociation. This is not surprising for X = Cl and Br due to low energy barriers (see Table 4.1). Although the energy requirements for C−I dissociation is large but still C−H dissociations were not observed for HICO. In a very small number of indirect trajectories, roaming of halogen atoms other than F was also observed. However, this fraction is very small due to the higher mass of halogens other than F. Roaming of halogen atoms in the gas phase dissociation of halons has been reported in a recent work [Godara and Paranjothy, 2019]. Zhao et al. [Zhao and Francisco, 1992] predicted in their electronic structure theory study that the gas phase Br + HCO reaction might occur via formation of excited HBrCO followed by concerted HBr + CO formation [Zhao and Francisco, 1992]. However, the present simulations indicate that the mechanism might involve direct abstraction of H by Br rather than the formation of stable HBrCO.

Snapshots of example trajectories showing different dissociation mechanisms of formyl halides along with relevant time evolved bond distances are presented in Figure 4.10. Each row shows snapshots of one trajectory and the right most panel shows C−H (black) and C−X (red) bond distances (in Å) as a function of time (in fs). The numbers inside the panels are time in fs at which the snapshot was taken. Rows (a) and (b) show HFCO trajectories resulting in HF + CO molecular products dissociating via radical recombinations with H and F migrations, respectively.

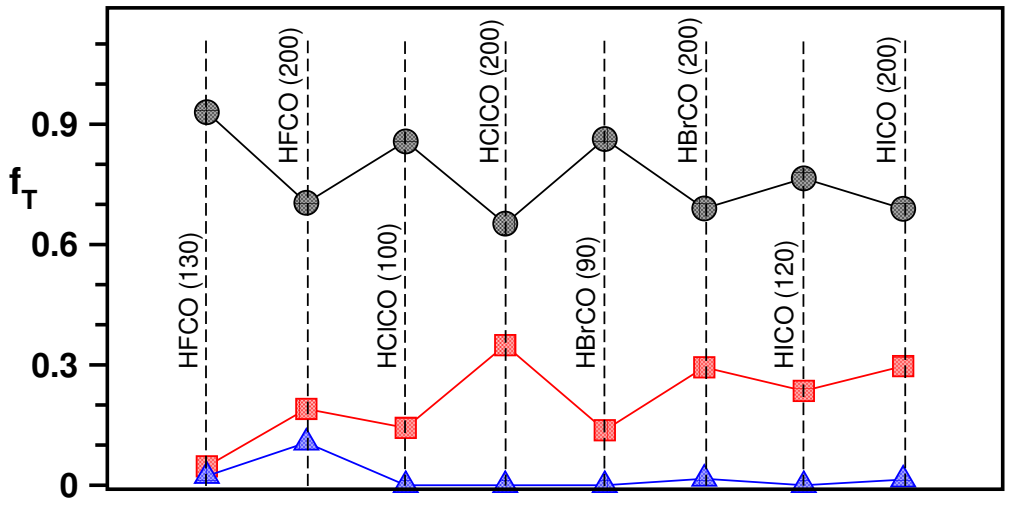

Figure 4.9. : Fraction of trajectories resulting in the HX + CO molecular products via concerted (black circles), isomerizations (blue triangles), and radical recombination (red squares) mechanisms. f_T is the ratio of number of trajectories dissociating via a given path and the total number of HX + CO forming trajectories.

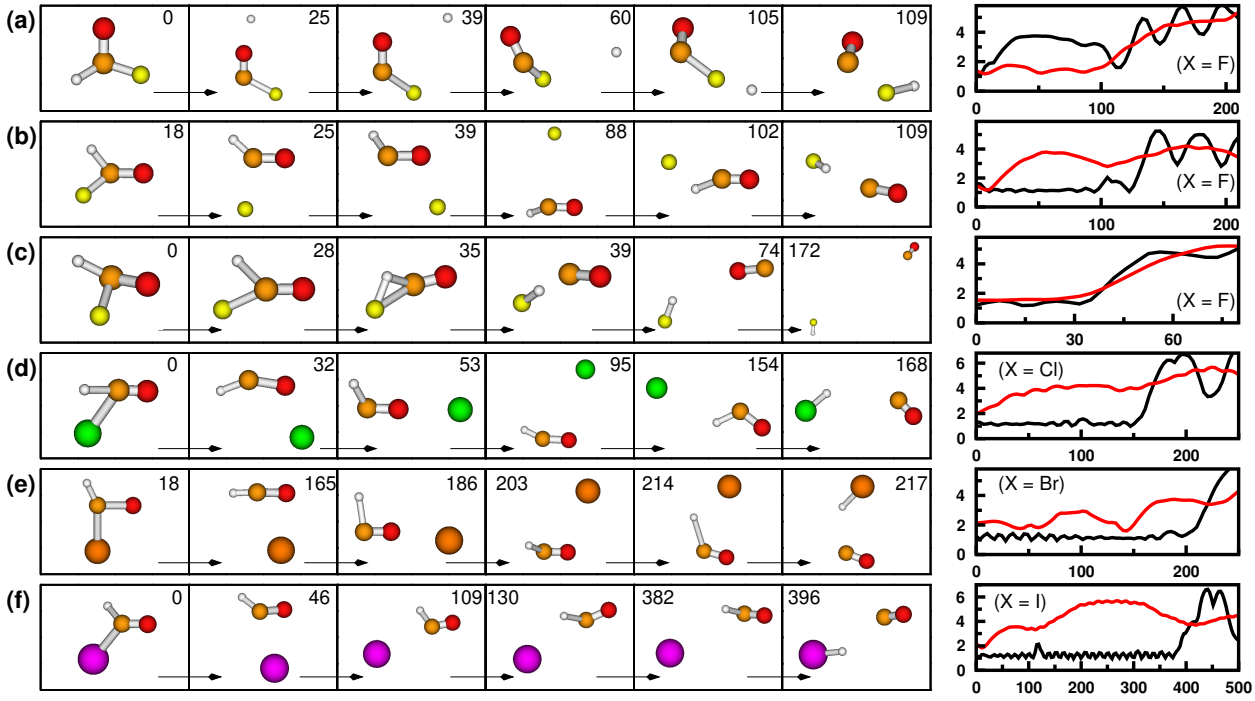

Figure 4.10. : Snapshots and bond distances of select trajectories are shown for the HXCO molecules. Each row shows snapshots of one trajectory and the right most panel in a given row shows C−H (black) and C−X (red) bond distances (in Å) as a function of time (in fs). The numbers inside each panel is time in fs at which the snapshot was taken. See text for details.

It can be observed from (a) that the dissociated H moves around the FCO species and comes back for F. This is also clearly seen in the corresponding bond distance plots. In the trajectory shown in (b), F dissociates and comes back for H. Figure 4.10(c) shows a HFCO concerted trajectory wherein the reaction step can be observed in the 35 fs frame. The time evolution of the bond distances in this trajectory are clearly distinct from the behavior observed in (a) and (b). In Figures 4.10(d), (e), and (f), indirect trajectories of HClCO, HBrCO, and HICO are shown wherein C−X dissociations and subsequent H abstractions by X can be seen. Clearly, the radical recombination mechanisms play an important role in the dissociation of formyl halides.

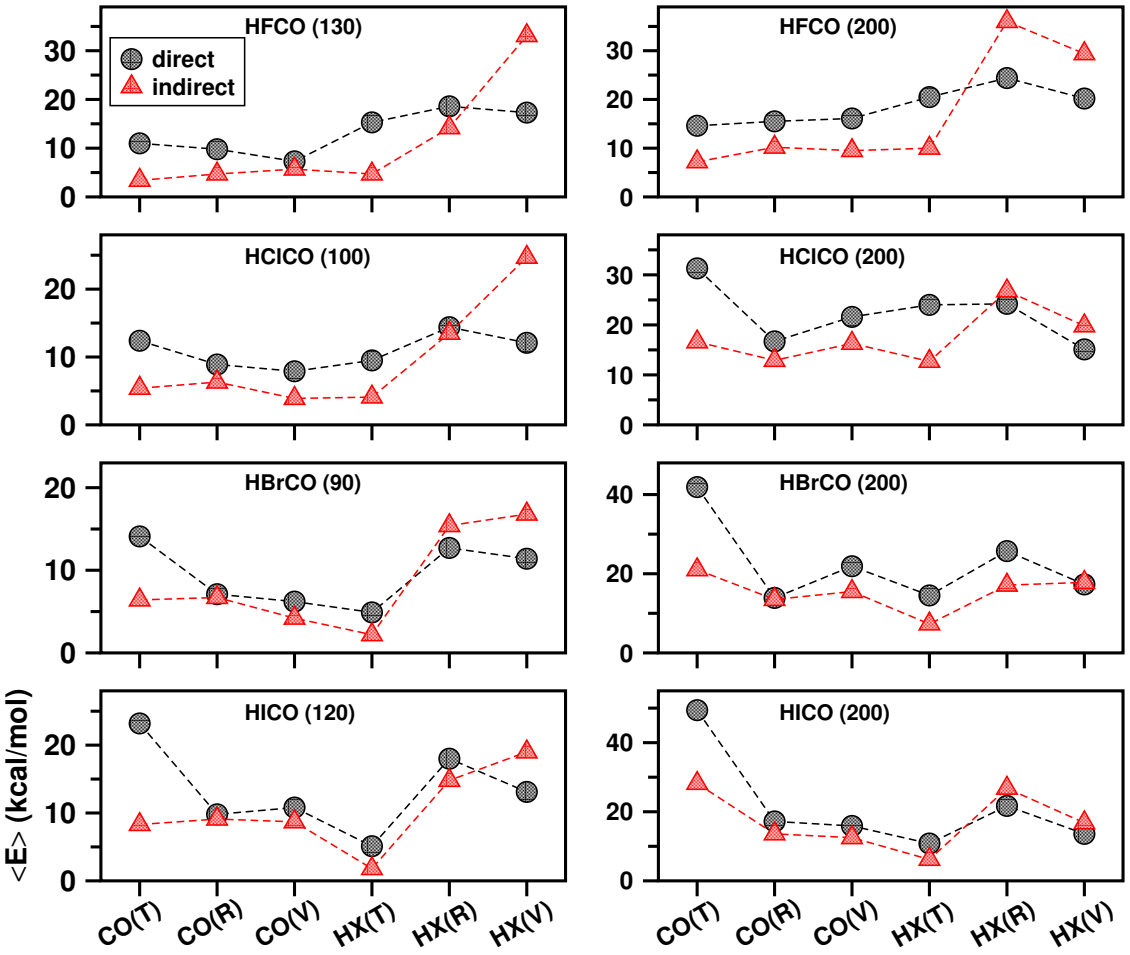

Figure 4.11. : Trajectory averaged translational (T), rotational (R), and vibrational (V) energies of CO and HX products resulting from direct (black circles) and indirect (red triangles) trajectories. x-axes are identical in all the plots wherein CO(T) corresponds to CO translational energy, etc. y-axes are trajectory averaged energies. Inside each panel, E_{tot} (in kcal/mol) is given in brackets.

Product energies were computed from the concerted and radical recombination trajectories resulting in HF + CO molecular products. Fraction of isomerization trajectories were small and they were not considered in calculating product energies. Direct dynamics method is computationally expensive and only a limited number of trajectories were available for computing product energies. Translational (T), rotational (R), and vibrational (V) energies of the HX + CO molecular products were computed from the simulations. The vibrational energy of a product is equal to the difference between the total energy of the product species and the corresponding translational and classical rotational energies [Hase, 2002]. The calculated energies were averaged

over trajectories and the results are summarized in Figure 4.11. Each panel in the figure shows data from one simulation wherein black circles and red triangles represent average energies from direct and indirect trajectories, respectively. CO(T) in the *x*-axes represent translational energy of CO molecule and so on.

Previous studies [Lahankar *et al.*, 2006; Zhang *et al.*, 2005] on formaldehyde dissociation have shown that the direct molecular pathway ($HCHO \longrightarrow H_2 + CO$) occurs via a concerted transition state (similar to TS-1 in Figure 4.3) and results in rotationally hot CO product in conjunction with vibrationally cold H_2. On the other hand, rotationally cold CO and vibrationally excited H_2 result from the roaming mechanism occurring via the $H_2CO \longrightarrow H + HCO$ radical formation followed by recombination. In the present work also, the direct and indirect trajectories give rise to different $HF + CO$ product energies as is evident from Figure 4.11. This difference is significant in the case of HFCO and HClCO. For HBrCO and HICO, the difference is noticeable only with the CO translational and HX vibrational energies. The present simulation results show that for HFCO and HClCO, (a) rotational energy of CO resulting from direct trajectories are slightly higher in comparison to that from indirect trajectories; (b) vibrational energy of HX from indirect trajectories are higher in comparison to that from direct trajectories. These trends are qualitatively same as those reported for the formaldehyde dissociation. Ishikawa et al. [Ishikawa *et al.*, 1984] reported observing high vibrational excitation of HF in comparison to CO in their infrared multi-photon dissociation study of HFCO which indicates that the HFCO might be dissociating via the indirect mechanism. For the HBrCO and HICO molecules, the situation is slightly different. The CO rotational energy from direct and indirect trajectories are almost same in both high and low energy simulations. However, the translational energy of the CO species in the direct trajectories increases. This is because the higher mass of the Br and I atoms and the C-X dissociation results in a larger momentum associated with the CO species. The HX vibrational energy is larger in the indirect trajectories in comparison to direct trajectories (the same trend as that of formaldehyde) in the low energy simulations whereas HX vibrational energies from the two types of trajectories are similar in the high energy simulations. Product energy distributions have not been reported previously in the literature for HBrCO and HICO. One common feature among the four molecules is that the translational energies of CO and HX products are higher in case of direct trajectories. This has been observed for X = F in a classical trajectory simulation reported by Yamamoto et al. [Yamamoto and Kato, 1997]. This can be understood by visualizing the motion of the normal mode associated with the corresponding reaction coordinate which shows that there is an impulsive force associated with the C−X dissociation. In the case of indirect trajectories, if the radical products had gained sufficient translational energy, they would separate and the subsequent abstraction reaction would not be possible.

4.2.3 Lifetime and RRKM Calculations

As mentioned earlier, incomplete IVR and mode specific effects were found [Yamamoto and Kato, 1997; Budenholzer and Yu, 1998] during the unimolecular dissociation of HFCO. To investigate the nature of intramolecular dynamics of formyl halides, lifetime distributions [Lourderaj and Hase, 2009] $N(t)/N(0)$ were computed from the direct dynamics trajectories. Here, $N(0)$ is the total number of trajectories and $N(t)$ is the number of trajectories that did not dissociate at time t. For RRKM unimolecular dynamics, the lifetime distribution is single exponential

$$N(t) = N(0)e^{-k(E)t} \tag{4.1}$$

where $k(E)$ is equal to the RRKM rate constant for an initial micro-canonical ensemble [Lourderaj and Hase, 2009]. For non-RRKM behavior, the initial $t = 0$ rate constant will be equal to

that of RRKM theory (due to the initial micro-canonical ensemble), but the ensuing dynamics will have rate constants smaller than those of the RRKM predictions. The lifetime distribution will be multi-exponential [Hase *et al.*, 1984]

$$N(t) = N(0)\sum_i f_i e^{-k_i t} \tag{4.2}$$

f_i is the fraction of the distribution dissociating with k_i, where $\sum_i f_i = 1$ [Sun *et al.*, 2012]. In Figure 4.12, lifetime distributions of formyl halides computed from trajectories (black circles) are shown along with RRKM theory predictions (blue lines). The harmonic RRKM rate constants were estimated [Zhu and Hase, 1994] using the electronic structure data computed with the B3LYP/6-31G*/ECP theory. $k_{\mathrm{RRKM}} = \sum_{i=1}^{5} k_i$ where k_1, k_2, etc., are rate constants for the five pathways shown in Figure 4.2. The radical paths (1) and (2) do not have saddle points and the corresponding rate constants were found variationally [Hase, 1983]. The trajectory data were fit to Eq. (4.1) or (4.2) and the fits are shown as red lines in Figure 4.12 and the fitted data are presented in Table 4.7. It can be observed from Table 4.7 that HFCO (200) and HBrCO (90), simulations showed strongest deviations from RRKM predictions. A sum of two exponentials were required to fit these data with significant contributions (f_1 and f_2) to both the components. The other simulations required two exponentials with one larger and one smaller component and not great variations in the rate constants. The only exception was HICO (120) simulation data which could be fit successfully with a single exponential. The classical harmonic RRKM theory rate constants, given in the last column of Table 4.7, are approximately 2 - 3 times larger than the rate constants extracted from trajectory simulations.

Table 4.7. : Values of k_i (in ps^{-1}) and f_i (Eq. (4.2)) fitted to trajectory lifetime data. k_{RRKM} is the harmonic RRKM rate constants computed from the electronic structure data. Simulation energy E_{tot} (in kcal/mol) is given in brackets.

	f_1	k_1	f_2	k_2	k_{RRKM}
HFCO (130)	0.04	5.86	0.96	4.98	12.64
HFCO (200)	0.70	17.31	0.30	6.56	49.20
HClCO (100)	0.04	0.95	0.96	6.16	12.89
HClCO (200)	0.01	1.21	0.99	26.39	70.76
HBrCO (90)	0.11	1.33	0.89	4.97	10.70
HBrCO (200)	0.29	24.99	0.71	25.92	78.40
HICO (120)	1.0	10.72	-	-	22.25
HICO (200)	0.21	28.96	0.79	29.47	66.91

The lifetime data presented here indicates, in general, that the intramolecular dynamics of formyl halides is non-statistical. In the present work, several trajectories underwent transition state recrossing violating one of the fundamental assumptions of RRKM theory and thus resulting in smaller rate constants than predicted by RRKM theory. Snapshots of example trajectories showing transition state recrossing are shown in Figures A.6(b), A.7(b), and A.8(b). It is important to note that the present dynamics simulations have shown roaming to be a possible dissociation mechanism of formyl halides and roaming dynamics in formaldehyde has been identified as non-statistical [Mauguière *et al.*, 2015].

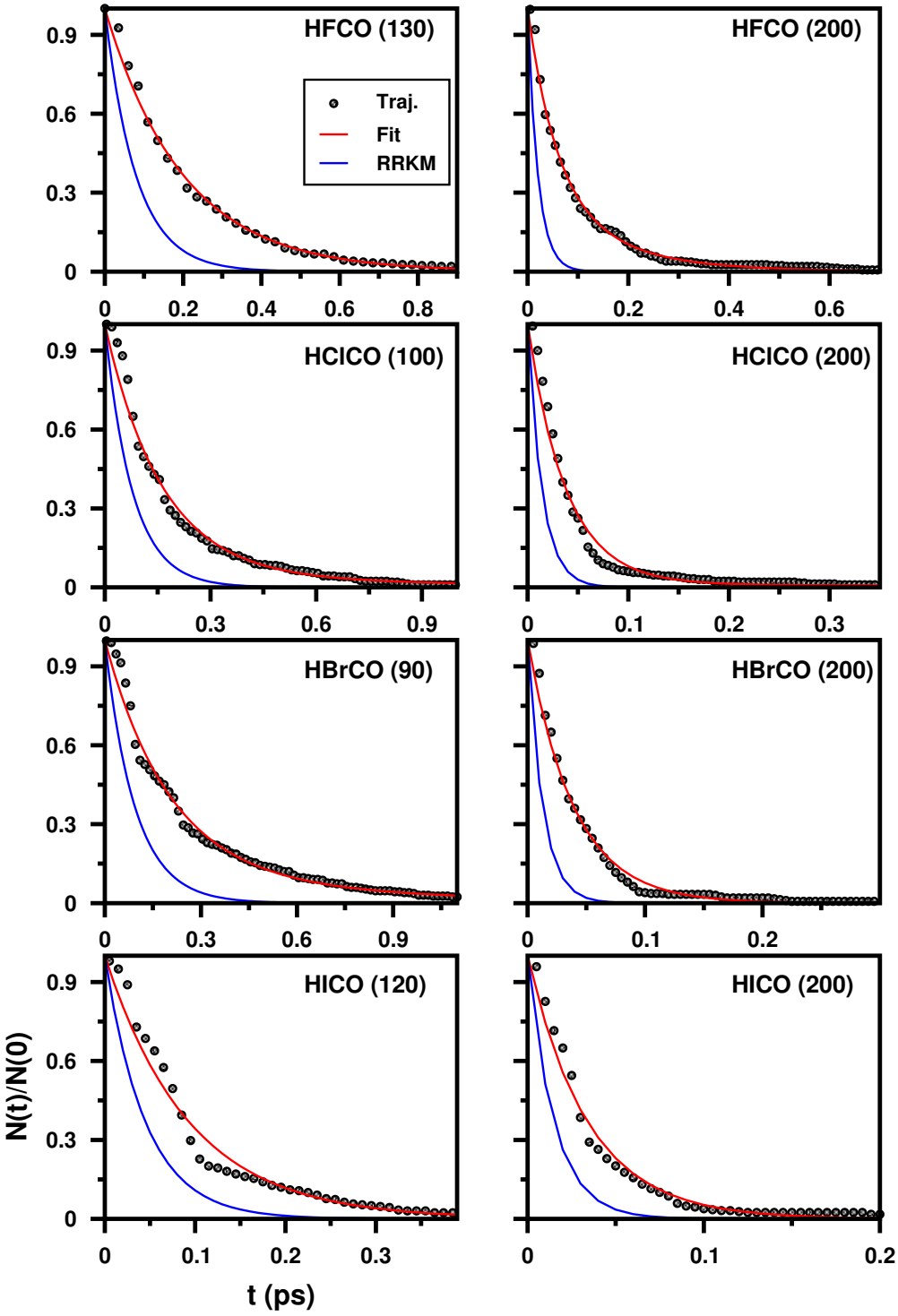

Figure 4.12. : Lifetime distributions $N(t)/N(0)$ estimated from trajectories (black circles) are given along with RRKM theory predictions (blue line). The red lines show fit of trajectory data to Eqs. (4.1) or (4.2) and the associated rate constants are given in Table 4.7. Inside each panel, E_{tot} (in kcal/mol) is given in brackets.

4.3 SUMMARY

The present work was motivated by the significance of gas phase dissociation of formyl halides in the atmosphere. Electronic structure calculations, classical direct dynamics simulations, and RRKM theory were used to investigate the reaction mechanisms and nature of intramolecular dynamics of formyl halides. The molecular products $HXCO \longrightarrow HX + CO$ can form via a concerted pathway and isomerization pathways involving 1,2-H and X shifts. Major fraction of the direct dynamics trajectories dissociated via the concerted pathway. Isomerizations have large energy requirements and only a small fraction of trajectories showed dissociation via isomerizations. The present simulations show that radical recombination reactions are important for the gas phase dissociation of formyl halides in addition to concerted and isomerization pathways. These indirect pathways have not been previously reported. A small fraction of trajectories showed roaming mechanisms involving both H and X. The $HX + CO$ product energies computed from concerted and radical recombination trajectories were in qualitative agreement with previous studies on formaldehyde dissociation. Further, the product energy distributions distinguish the two types of mechanisms. An important result from the present study is that the radical pathways are competitive with the HX + CO molecular product formation. Previous studies on formyl halides have focused primarily on the molecular product formation. Dissociation products of formyl halides such as HX, X, and XCO play a significant role in ozone layer depletion and thus have a significant influence on the chemical composition of the troposphere [Simpson *et al.*, 2015]. In the work presented here, reaction mechanisms were studied in detail but the nature of IVR dynamics has not been completely established. Previous studies [Yamamoto and Kato, 1997; Budenholzer and Yu, 1998] on HFCO and the present investigation has pointed towards non-statistical energy flow dynamics in formyl halides and this needs to be investigated further.

…